JOURNAL OF GEOPHYSICAL RESEARCH, VOL. 101, NO. D21, PAGES 26,333–26,346, NOVEMBER 27, 1996

Causal space-time multifractal processes: Predictability and forecasting of rain fields

David Marsan and Daniel Schertzer
Laboratoire de Météorologie Dynamique, Université Pierre et Marie Curie, Paris, France

Shaun Lovejoy
Physics Department, McGill University, Montreal, Canada

Abstract. Building on earlier cascade models of rainfall, we propose a model of space-time rain fields based on scaling dynamics. These dynamics are indeed related to the space-time symmetries of the turbulent medium within which rainfall occurs: the underlying phenomenology corresponds to a cascade of structures with lifetimes depending only on the scale of the structures. In this paper we clarify two major issues: the scaling anisotropy between space and time, and the need to respect causality, i.e., a fundamental asymmetry between past and future. We detail how this "arrow of time" breaks the mirror symmetry with respect to the spatial hyperplane, and how it can be introduced in continuous multiplicative cascade models so as to remove the artificial temporal mirror symmetry of earlier models. We show that such a causal multifractal field can be understood as the result of an anomalous diffusion acting on the singularities of the field. Finally we will exploit and test these models through (1) a succinct analysis of rainfall data, (2) numerical simulations of the temporal decorrelation of two initially similar fields (accounting for the loss of predictability of the process), and (3) a forecasting method for multifractal rain fields.

1. Introduction

In recent years, there has been considerable development of multifractal techniques for treating rain fields in a multifractal framework (see *Lovejoy and Schertzer* [1995] for a recent review). Indeed, they allow one to overcome the severe limitations of the two primary approaches to rainfall modeling: the phenomenological stochastic modeling favored by the hydrologists, and the deterministic dynamical modeling favored by the meteorologists.

The stochastic approaches were largely ad hoc; they were designed to mimic the rain phenomenology [*Austin and Houze*, 1972] and were based on the assumption that rain processes are qualitatively different over every factor of 2 or so in scale. The scientific outcome of relying on this phenomenology has been a series of very complex cluster processes whose hierarchies of time scales and space scales are each assigned plausible variations in rain rate and statistical fluctuations. For instance, the well-known Waymire-Gupta-Rodriguez-Iturbe (WGR) model [*Waymire et al.*, 1984] involves a dozen or so empirical parameters and is at best successful only within the narrow range of time scales and space scales for which it was calibrated.

In contrast, the deterministic models were developed following the usual methods of geophysical fluid dynamics and largely based on various truncations of the Navier-Stokes equations. They are predicated on the integration of nonlinear partial differential equations which attempt to represent the complex nonlinear dynamics hopefully including appropriate parametrizations of the physics. Because of the limited number of degrees of freedom which can be explicitly modeled, this approach makes drastic scale truncations, typically studying one scale independently of the others, transforming partial differential equations (PDE), into ordinary differential equations (ODE), arbitrarily hypothesizing the homogeneity of subgrid-scale fields, and performing ad hoc parameterizations. Even if one ignores these oversimplifying assumptions, the consequences of such choices, which have increasingly weak links with the real world, are ultimately complex and unwieldy numerical codes.

In order to overcome the limitations of both conventional approaches and to bridge the gap between them, it was argued [*Schertzer and Lovejoy*, 1987a] that physically based models involving huge ratios of scale and intensity could be developed, with the help of multiplicative cascade models [*Yaglom*, 1966; *Mandelbrot*, 1974; *Schertzer and Lovejoy*, 1984; *Kahane*, 1985; *Pietronero*

Paper number 96JD01840.
0148-0227/96/96JD-01840$09.00

and Siebesma, 1986; *Meneveau and Sreenivasan*, 1987]. Indeed, by avoiding truncations of the dynamical equations, cascades preserve the fundamental dynamical scaling symmetries. With a unique exception, the so-called β model [*Novikov and Stewart*, 1964; *Frisch et al.*, 1978], these cascades yield fields with infinite hierarchies of singularities [*Schertzer and Lovejoy*, 1984; *Benzi et al.*, 1984; *Parisi and Frisch*, 1985; *Halsey et al.*, 1986] and associated dimensions [*Hentschel and Procaccia*, 1983; *Grassberger*, 1983], and therefore multifractal fields rather than fractal sets [*Mandelbrot*, 1982].

However, most of the applications to rain were unfortunately perceived as dealing either with one-dimensional (1-D) time series of rain rates estimated by rain gauges, especially for data analysis, or two-dimensional (2-D) and three-dimensional (3-D) radar images. So far, very limited attention has been devoted to scaling space and time rain processes (see, however, *Lovejoy and Schertzer* [1991], *Brenier et al.* [1991] and *Tessier et al.* [1993]; see also *Lovejoy and Mandelbrot* [1985] and *Lovejoy and Schertzer* [1985] for monofractal modeling); this strong limitation leads to incomplete and inadequate analyses, especially when considering important issues such as forecasting, which need to be formulated in a space-time framework, or space-time sampling strategies.

In *Schertzer and Lovejoy* [1987a] it was argued that, although rain fields are certainly non passively advected by atmospheric turbulence, to investigate the case of a passive scalar undergoing advection corresponding to the Navier-Stokes equations is already a fundamental and yet not trivial issue. Moreover it is expected, as shown by numerous analyses [*Schertzer and Lovejoy*, 1985; *Lovejoy and Schertzer*, 1991; *Pflug et al.*, 1993; *Tessier et al.*, 1993], that the scaling symmetries in space and time arising from the Navier-Stokes equations at large Reynolds numbers, thus characterizing atmospheric turbulence, should lead to a similar scaling behavior for active scalar fields such as rain (or clouds, for a related example).

2. The Anisotropic Space-Time Scaling of Turbulence

We first recall the formal argument for scaling based directly on the scaling properties of the incompressible Navier-Stokes equations:

$$\partial_t \underline{u} + (\underline{u}.\underline{\nabla})\underline{u} = -\frac{1}{\rho_f}\underline{\nabla} p + \nu \triangle \underline{u} \; ; \; \nabla \underline{u} = 0 \qquad (1)$$

where $\underline{u}$ is the velocity, ρ_f the fluid density, p the pressure and ν the kinematic viscosity. At large Reynolds numbers the scaling symmetries can be deduced from the action of the "scale changing" operator $T_\lambda : \underline{x} \mapsto \underline{x}/\lambda$; the invariance of the Navier-Stokes equation (1) under this operation leads to the following scaling laws:

$$t \mapsto t/\lambda^{1-H} \qquad (2)$$

$$\underline{u} \mapsto \underline{u}/\lambda^{H} \qquad (3)$$

$$\nu \mapsto \nu/\lambda^{1+H} \qquad (4)$$

and the pressure has been removed by projection on the divergence-free plane. The associated equation for a passive scalar (of concentration ρ),

$$\partial_t \rho + \underline{u}.\underline{\nabla}\rho = \kappa \triangle \rho \qquad (5)$$

where κ is the molecular diffusivity, gives, following the same argument,

$$t \mapsto t/\lambda^{1-H} \qquad (6)$$

$$\rho \mapsto \rho/\lambda^{H'} \qquad (7)$$

$$\kappa \mapsto \kappa/\lambda^{1+H} \qquad (8)$$

Here, we are mainly interested in the resulting symmetries for space, $l \mapsto l/\lambda$, and time, $t \mapsto t/\lambda^{1-H}$. It must be noted that the exponent H is unknown a priori, $H \neq 0$ resulting in a scaling anisotropy between space and time. This anisotropy will be discussed below in more details, using the generalized scale invariance (GSI) framework (see below for references on GSI).

The Kolmogorov scaling for the velocity field [*Kolmogorov*, 1941; *Obukhov*, 1941] and the Corrsin-Obukhov scaling for the passive scalar [*Obukhov*, 1949; *Corrsin*, 1951] are classically obtained by considering homogeneous fluxes of energy ϵ (the relevant quantity being thus the spatially averaged energy flux $\bar{\epsilon}$), or scalar variance in the case of a passive scalar. These dimensional arguments lead to the scaling relation for the characteristic lifetime (turnover time) τ_l of an eddy or a scalar blob at scale l,

$$\frac{1}{\tau_l} \sim \frac{\bar{\epsilon}}{\delta u_l^2} \sim \frac{\bar{\epsilon}}{\bar{\epsilon}^{\frac{2}{3}} l^{\frac{2}{3}}} \qquad (9)$$

and thus,

$$\frac{1}{\tau_l} \sim \bar{\epsilon}^{\frac{1}{3}} l^{-\frac{2}{3}} \qquad (10)$$

For inhomogeneous turbulence [*Kolmogorov*, 1962; *Obukhov*, 1962] the same arguments lead to the multiscaling relation:

$$\frac{1}{\tau_l} \sim \epsilon_l^{\frac{1}{3}} l^{-\frac{2}{3}} \qquad (11)$$

where we now consider the inhomogeneous energy flux field ϵ_l at all scales l. The scaling anisotropy exponent H such that $1 - H = \frac{2}{3} \Rightarrow H = \frac{1}{3}$ is thus expected to characterize atmospheric turbulence. As argued above, we claim that these symmetries will hold for rain fields, though not necesserily with the same exponents; however, even if most of the further developments will be derived using an a priori unknown H, we will test the theory, for illustrative purposes, taking $H = \frac{1}{3}$. Note that *Lovejoy and Schertzer* [1991] directly estimated $H = 0.5 \pm 0.3$ for raindrops.

It is important to stress that a direct consequence of this scaling relation between space and time is the

absence of a global characteristic time for the system (since there is no characteristic length in a process possessing scaling properties); we thus expect an algebraic decorrelation in time for the singularities of the field. This is a very distinctive feature of stochastic cascade models when compared to deterministic chaos, which instead predicts an exponential decorrelation: for low-dimensional, nonlinear systems, two initially nearby phase-space trajectories diverge exponentially with time, this divergence being characterized by the Liapunov exponent, which is the inverse characteristic time, of the system. This difference between these two types of system arises from the fact that deterministic chaotic systems possess only a few degrees of freedom, contrary to stochastic systems with many degrees of freedom, involving a wide range of dynamically significant scales.

In developing multiplicative cascades both in time and space, two main difficulties arise, with respect to isotropic, plane-symmetrical multifractal processes: (1) the scaling anisotropy due to the exponent H which is a priori different from 0, and (2) the need for the process to be causal, i.e., the symmetry breaking along the time axis, necessary in order to allow one to distinguish between past and future (whereas statistical isotropy in space is legitimately considered).

In section 3 we study the rather pedagogical case of discrete multiplicative cascade models as a natural consequence of the phenomenology underlying the Kolmogorov and Corrsin-Obukhov scaling. The scaling anisotropy is introduced, and we derive a (generalized) correlation function for these models, showing clearly the algebraic decorrelation both in space and time. The main part of this article is devoted, in section 4, to the transformation of the more sophisticated continuous cascade models to account for the "time arrow", or causality. It is shown that causality is respected as soon as one considers the dynamics of the singularities of the field; more precisely, a causal multifractal field corresponds to the result of an anomalous diffusion process acting on the singularities. In section 5 we present and discuss the preliminary results of an analysis performed on the U.S. composite rainfall data sets derived from National Weather Service (NWS) Radars data (NOWrad, registered trademark of WSI Corporation). This analysis indicates that the observed rainfall field is indeed the result of a space-time multiplicative cascade. Finally, in section 6, we investigate how these models can provide a pertinent framework in order to simulate the decorrelation of a perturbed field with its nonperturbed image; we then propose a physically based forecast method for multifractal processes, this application being one of the basic motivations of this work.

3. Discrete Cascades

The simplest multifractal models are multiplicative discrete cascades. We first recall how such cascades are generated, and we determine a generalized correlation function. We first restrict ourselves to an exclusively spatial model, i.e., without a time coordinate, by considering an isotropic 2-D space. We denote by L the length of our square domain where the cascade will be developed; the first step of the cascade is done by dividing this square into $\lambda \times \lambda$ (λ is an integer) structures of equal size $l_1 = L\lambda^{-1}$. We consider a random variable $\mu\epsilon$ such that $Pr(\mu\epsilon < 0) = 0$ (Pr indicates "probability") and $\langle \mu\epsilon^q \rangle = \lambda^{K(q)}$; we use realizations $\mu\epsilon_i(\underline{x})$ of $\mu\epsilon$ that are all statistically independent of each other (i.e. with respect to scale index i and spatial coordinate $\underline{x}$). The structures at scale l_1 are given intensity values $\epsilon_1(\underline{x}) = \mu\epsilon_1(\underline{x})$ (since we have $\lambda \times \lambda$ structures, only $\lambda \times \lambda$ independent realizations are used). At each following step of the cascade we divide the structures at scale $l_n = L\lambda^{-n}$ into $\lambda \times \lambda$ new structures at scale $l_{n+1} = L\lambda^{-(n+1)}$, and give them intensities such that

$$\epsilon_{n+1}(\underline{x}) = \mu\epsilon_{n+1}(\underline{x}) \cdot \epsilon_n(\underline{x}) \tag{12}$$

In this cascading process, we thus see that neighboring structures at any given scale are indeed offspring of a common ancestor at the previous scale.

Now, in order to generate cascades in a space-time domain, and due to the scaling anisotropy between space and time, we need to proceed to a slightly different kind of construction, the simplest case treated in the GSI framework, or self-affine instead of self-similar cascades. We consider that one axis corresponds to the spatial coordinate, while the other is for the time coordinate; in order to introduce the scaling anisotropy between space and time (given by the exponent H), we change each cascade step by dividing the structures at scale $l_n = L\lambda^{-n}$ into λ (along the spatial axis) $\times\lambda^{1-H}$ (along the temporal axis) new structures at scale $l_{n+1} = L\lambda^{-(n+1)}$, still with λ and λ^{1-H} integers. For $H = \frac{1}{3}$, the smallest allowable λ is $\lambda = 8$, which gives $\lambda^{\frac{2}{3}} = 4$. Note that $\lambda = 3$ and $\lambda^{1-H} = 2$ gives $H = 0.37$, which is an acceptable approximation of $H = \frac{1}{3}$.

Figure 1 shows such a discrete cascade developed on a set of seven scales, with $\lambda = 3$ and $H = 0.37$, the horizontal and the vertical axis corresponding to t and x, respectively. Here we took $\mu\epsilon$ lognormal. Figure 2 shows three sections of this field along the temporal axis, at different spatial locations. We see that the three sections are stationarily correlated to each other, and that this correlation decreases as the interval $|\Delta x|$ between the sections increases.

These models of self-affine discrete cascades already reproduce the phenomenology of turbulent cascades; in this scheme, each spatial structure, or eddy, confined at a given scale l is given a lifetime τ_l depending only on its scale: $\tau_l \sim l^{1-H}$. When this time has expired, a new structure is created as the direct offspring of its parent structure. This time scale also corresponds to the time necessary for all the offspring structures from scale l down to the smallest scale to be replaced by new structures.

At this point, it is interesting to determine a generalized (involving moments of arbitrary order q_1 and q_2)

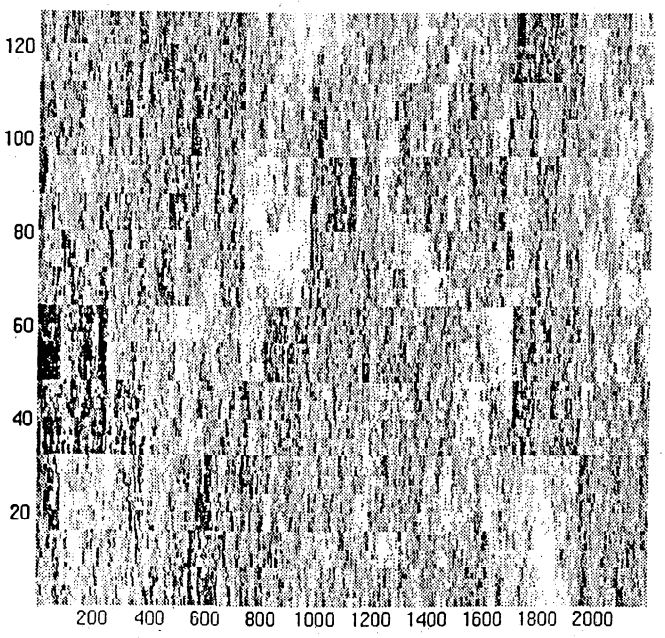

Figure 1. Realization of a discrete cascade developed on seven generating steps. Parameters are $\lambda = 3$, $H = 0.37$, and $\mu\epsilon$ is a lognormal random variable of mean 1 and covariance 0.1. The x coordinate is along the vertical axis, the t coordinate is along the horizontal axis. We display here the logarithm of the field; the intensity scale is linear.

correlation function for our process:

$$\mathcal{J}_n^{(q_1,q_2)}(|\Delta\underline{x}|,\Delta t) = \langle \epsilon_n^{q_1}(\underline{x},t)\,\epsilon_n^{q_2}(\underline{x}+\Delta\underline{x},t+\Delta t)\rangle \quad (13)$$

We first derive it in the simple case of a 2-D cut of an isotropic spatial cascade. Two structures (at scale l_n) separated by $|\Delta\underline{x}|$ (with $|\Delta\underline{x}| > l_n$) are offspring of the same parent structure at scale l_m, such that

$$l_m = |\Delta\underline{x}| \quad (14)$$

(this equality is generally true, i.e., a small discrepancy can appear owing to the arbitrary discreteness of the set of cascading steps; however, this discrepancy disappears in the more general framework of continuous cascades). Thus the intensities of these two structures correspond to the same cascade developed from L down to l_m, and afterwards to independent cascades from l_m to l_n. Then

$$\epsilon_n(\underline{x}) = \epsilon_m(\underline{x}) \prod_{i=m+1}^{n} \mu\epsilon_i(\underline{x}) \quad (15)$$

$$\epsilon_n(\underline{x}+\Delta\underline{x}) = \epsilon_m(\underline{x}) \prod_{i=m+1}^{n} \mu\epsilon_i(\underline{x}+\Delta\underline{x}) \quad (16)$$

where all $\mu\epsilon$ are independent of each other. Thus

$$\mathcal{J}_n^{(q_1,q_2)}(|\Delta\underline{x}|) \sim \langle \epsilon_m^{q_1+q_2}(\underline{x})\rangle \langle \prod_{i=m+1}^{n} \mu\epsilon_i^{q_1}(\underline{x})\rangle \langle \prod_{i=m+1}^{n} \mu\epsilon_i^{q_2}(\underline{x}+\Delta\underline{x})\rangle \quad (17)$$

gives

$$\mathcal{J}_n^{(q_1,q_2)}(|\Delta\underline{x}|) \sim \langle \mu\epsilon^{q_1+q_2}\rangle^m \langle \mu\epsilon^{q_1}\rangle^{n-m} \langle \mu\epsilon^{q_2}\rangle^{n-m} \quad (18)$$

and finally,

$$\mathcal{J}_n^{(q_1,q_2)}(|\Delta\underline{x}|) = l_n^{-[K(q_1)+K(q_2)]} |\Delta\underline{x}|^{K(q_1)+K(q_2)-K(q_1+q_2)} \quad (19)$$

We refer the reader to papers devoted to such two-point correlation functions (see, for example, *Cates and Deutsch* [1987], *O'Neil and Meneveau* [1993], or the derivation in *Monin and Yaglom*, [1975, vol. 2, pp. 618-620], in the case of lognormal multifractals).

We now extend the generalized correlation function to space-time intervals $(\Delta\underline{x}, \Delta t)$. For spatial intervals $(\Delta\underline{x}, 0)$, one recovers the results detailed above. For temporal intervals $(0, \Delta t)$, the same derivation can be developed simply by changing equation (14) into

$$l_m = |\Delta t|^{\frac{1}{1-H}} \quad (20)$$

After some algebra, we obtain

$$\mathcal{J}_n^{(q_1,q_2)}(\Delta t) \sim l_n^{-[K(q_1)+K(q_2)]} |\Delta t|^{\frac{1}{1-H}[K(q_1)+K(q_2)-K(q_1+q_2)]} \quad (21)$$

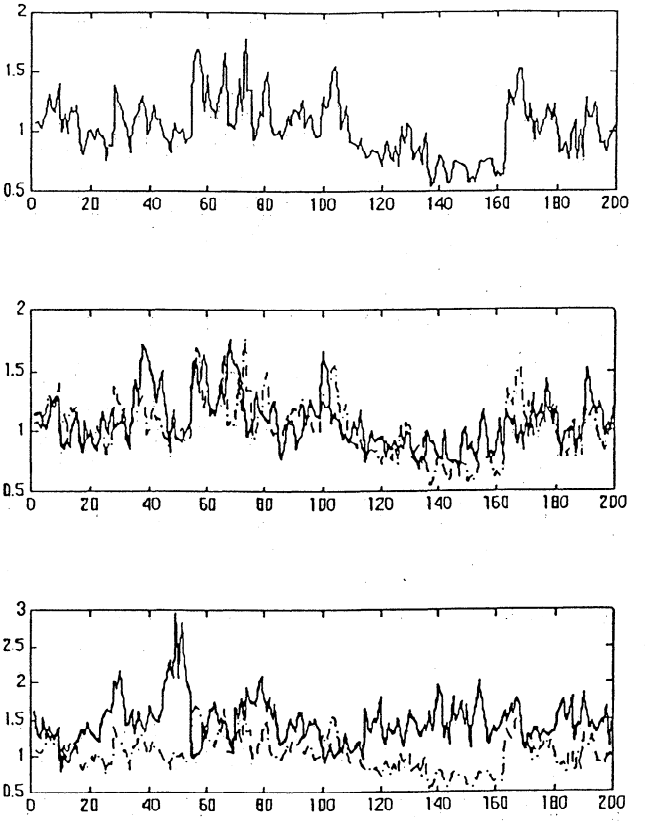

Figure 2. Three sections along the t axis of the cascade displayed in Figure 1. The three sections correspond (from top to bottom) to $x = 10$, $x = 14$, and $x = 30$. For comparison, the last two are shown along with the section at $x = 10$ (dashed lines).

Defining a scale function in the 2-D space-time domain by $||(\underline{x},t)|| = \max\{|\underline{x}|, t^{\frac{1}{1-H}}\}$, where $\underline{x}$ and t have been non-dimensionalized by dividing them with the integral scale/time, respectively, we finally obtain

$$\mathcal{J}_n^{(q_1,q_2)}(\Delta\underline{x},\Delta t) \sim l_n^{-[K(q_1)+K(q_2)]} ||(\Delta\underline{x},\Delta t)||^{K(q_1)+K(q_2)-K(q_1+q_2)} \quad (22)$$

which clearly shows that the correlation is algebraic both in the spatial and temporal directions, with an anisotropy exponent H.

One can easily perceive some limitations in this kind of model; the causal properties are not explicitly detailed, though the corresponding phenomenology seems indeed to be appropriate in that respect. The temporal modulations of the structures at a given scale occur at the same time for all of them; this limits the possible exploitation of these models, especially for forecasting. We thus need to reformulate the problem by considering the more sophisticated framework of continuous cascades, where "continuous" refers to a continuous ensemble of scales (and not only a crude discrete set as above). Instead of generating a cascade by multiplying independent factors at each step, one can define a multifractal field starting from a white noise field regular/homogeneous at the smallest scale. By doing this, we will be able to define a cascade process giving birth to a causal multifractal field.

4. Continuous Cascades

Continuous cascade models have the major advantage of developing cascades over a continuous interval of scales instead of only a discrete set [*Schertzer and Lovejoy*, 1987b, 1991, 1992; *Wilson et al.*, 1991; *Pecknold et al.*, 1993]. Moreover, as can be clearly observed in Figure 1, discrete cascades have the disadvantage of creating artificial rectangles, this being due to the process that divides a rectangular structure into smaller rectangular structures, following a self-affine process. We will briefly present here the basic ingredients of this improved method, first, for the specific and simplest case of spatial isotropic multifractal fields; then we will devote a short section to (still spatial) anisotropic fields, giving a succinct summary of important GSI notions. Then we will consider the original case of causal anisotropic processes. Note that anisotropic space-time multifractals were already evoked by *Brenier et al.* [1991] and *Lovejoy and Schertzer* [1991] and briefly discussed by *Tessier et al.* [1993] using the GSI framework; moreover, in the latter papers, analyses of the anisotropy between time and a spatial coordinate for a set of lidar and radar scans were performed.

Construction of a Spatial Isotropic Field

Instead of considering multiplications of random fields, it is simpler to generate continuous cascades by considering an additive process for the logarithm of the field. We thus define the generator Γ_λ at resolution $\lambda = L/l$ of the multifractal field ϵ_λ: $\epsilon_\lambda = e^{\Gamma_\lambda}$ (the notation ϵ_n used for the discrete cascades is here changed into ϵ_λ where the resolution λ is a continuous parameter). In order for ϵ_λ to be multifractal, we need its q-order moments to follow an algebraic law with respect to scale:

$$\langle \epsilon_\lambda^q \rangle \sim \lambda^{K(q)} \Rightarrow \langle e^{q\Gamma_\lambda} \rangle \sim e^{K(q)\log\lambda} \quad (23)$$

We thus see that the (second) Laplace characteristic function of Γ_λ, i.e. $\log\langle\exp(q\Gamma_\lambda)\rangle$, should diverge logarithmically with the resolution.

From here on we will consider universal multifractal fields, i.e. such that the moment scaling function $K(q)$ verifies $K(q) = \frac{C_1}{\alpha-1}(q^\alpha - q)$ where C_1 is the codimension of the mean singularity, and α is the Lévy index characteristic of the field; the generator is thus the infinite limit of the sum of independent stable (Lévy) random variables. We compute the generator starting from a white Lévy noise γ_λ, the subgenerator, of Lévy index α smoothed at resolution λ, by a fractional integration of order h:

$$\Gamma_\lambda(\underline{x}) = g_\lambda(\underline{x}) \star \gamma_\lambda(\underline{x}) \quad (24)$$

where $g_\lambda(\underline{x}) \sim |\underline{x}|^{-h}$ is band-limited to $|\underline{k}| \in [1/L; \lambda/L]$ (and $\star$ is the convolution product). The derivation given in Appendix A shows that

$$\langle e^{q\Gamma_\lambda} \rangle = \exp[q^\alpha \int_{\frac{L}{\lambda}}^{L} d\underline{x}\ |\underline{x}|^{-\alpha h} + q\gamma_0] \quad (25)$$

where γ_0 is a recentering term constrained by $K(1) = 0$ (see *Pecknold et al.* [1993] for numerical implementation). In order to get the expected logarithmic divergence in λ,

$$\int_{\frac{L}{\lambda}}^{L} d\underline{x}\ |\underline{x}|^{-\alpha h} \sim \log\lambda \quad (26)$$

we need

$$|\underline{x}|^{-\alpha h} \sim |\underline{x}|^{-d} \quad (27)$$

where d is the dimension of space; we thus get

$$h = \frac{d}{\alpha} \quad (28)$$

We then see that, by taking the exponential of a Lévy white noise of Lévy index α integrated fractionally (of order d/α) on the range $[1/L; \lambda/L]$, we generate a log-Lévy multifractal field resulting from a continuous cascade process from scale L down to scale l. Again, for a more detailed and algorithmic description of this construction, we refer the reader to, for example, *Pecknold et al.* [1993].

Self-Affinity

Anisotropy arises when the scale changing operator T_λ acts differently in different directions. The simplest case corresponds to self-affinity, and since we predict our cascade process to be self-affine with space and time coordinates, we will limit ourselves to this. However more involved cases can be equivalently treated [*Lovejoy*

and Schertzer, 1985; *Schertzer and Lovejoy*, 1985, 1989; *Lovejoy et al.*, 1992; *Pflug et al.*, 1993; *Pecknold et al.*, 1996].

Consider the scale changing operator T_λ acting on a two-dimensional spatial domain:

$$T_\lambda : \begin{pmatrix} x \\ y \end{pmatrix} \mapsto \lambda^{-\mathcal{G}} \begin{pmatrix} x \\ y \end{pmatrix} \tag{29}$$

with

$$\mathcal{G} = \begin{pmatrix} 1 & 0 \\ 0 & 1-H \end{pmatrix} \tag{30}$$

The field ϵ_λ is then anisotropic with "elliptical dimension" $d_{\rm el} = Tr\,\mathcal{G} = 2-H$ if it follows scaling laws under the action of T_λ:

$$\epsilon_{\lambda'} \equiv \epsilon_\lambda(T_\lambda[\epsilon_{\lambda'/\lambda}]) \tag{31}$$

where $\equiv$ denotes statistical identity, and $T_\lambda[f(\underline{x})] = f(T_\lambda[\underline{x}])$. It then follows that the iso-correlation curves of the field define a family globally invariant under T_λ. Their exact shape does not matter; only their scale is of importance.

In order to generate such an anisotropic field, we thus need an anisotropic filter $g_\lambda(\underline{x})$, such that

$$g_\lambda(T_\Lambda[\underline{x}]) \sim \Lambda^{-h}\, g_\lambda(\underline{x}) \tag{32}$$

This can be achieved by defining the scale function $||\underline{x}||$:

$$g_\lambda(\underline{x}) \sim ||\underline{x}||^{-h} \tag{33}$$

and $||\underline{x}||$ has the property

$$||T_\lambda[\underline{x}]|| = \lambda^{-1}||\underline{x}|| \tag{34}$$

For example, given the diagonal matrix $\mathcal{G}$ introduced above, we can choose either $||\underline{x}|| = |x| + |y|^{\frac{1}{1-H}}$, $||\underline{x}|| = (x^2 + (y^2)^{\frac{1}{1-H}})^{1/2}$, or $||\underline{x}|| = \max\{|x|, |y|^{\frac{1}{1-H}}\}$ as already seen above. This arbitrariness in the choice of this scale function is a consequence of the arbitrariness on the shape of the isocorrelation curves. Note that the band limitation of g_λ corresponds now to $||\underline{x}|| \in [L/\lambda; L]$.

Causality

In order to define a causal process in space and time, we need to perform a causal filtering of the subgenerator γ_λ, i.e., to work with g as a retarded Green function, whereas, in the preceding sections, we were considering only noncausal fields, i.e., with a mirror symmetry with respect to the spatial hyperplane. Equation (24), rewritten as a differential equation,

$$g_\lambda^{(-1)}(|\underline{x}|, t) \star \Gamma_\lambda(\underline{x}, t) = \gamma_\lambda(\underline{x}, t) \tag{35}$$

(where the Fourier transform of $g^{(-1)}$ is the inverse of the Fourier transform of g) is now expected to correspond to a diffusion equation (which might be anomalous; see below), with the subgenerator γ_λ providing the forcing. A causal Γ_λ will result if the temporal part of $g^{(-1)}$ involves operators such as ∂_t or the causal fractional derivative of order ζ: ∂_{t^ζ}.

By inverting the action of g in equation (35), equation (24) is then changed to

$$\Gamma_\lambda(\underline{x}, t) = \int_{-\infty}^{t} dt' \int_{-\infty}^{+\infty} d\underline{x}'\; g_\lambda(|\underline{x} - \underline{x}'|, t - t')\; \gamma_\lambda(\underline{x}', t') \tag{36}$$

which is obviously causal since the convolution is performed only on the part of the subgenerator corresponding to the past ($t' < t$). This can be rewritten, introducing the Heaviside distribution $\Theta(t)$, as

$$\Gamma_\lambda(\underline{x}, t) = [g_\lambda(|\underline{x}|, t)\; \Theta(t)] \star \gamma_\lambda(\underline{x}, t) \tag{37}$$

We thus define the retarded Green function $g_\lambda^{\rightarrow}(|\underline{x}|, t)$ by

$$g_\lambda^{\rightarrow}(|\underline{x}|, t) \;=\; g_\lambda(|\underline{x}|, t)\; \Theta(t) \tag{38}$$

or equivalently,

$$\hat{g}_\lambda^{\rightarrow}(|\underline{k}|, \omega) \;=\; \hat{g}_\lambda(|\underline{k}|, \omega) \star \hat{\Theta}(\omega) \tag{39}$$

where

$$\hat{\Theta}(\omega) = \frac{1}{2}\delta(\omega) + \frac{i}{2\pi} p.v.\frac{1}{\omega} \tag{40}$$

$p.v.$ stands for the Cauchy principal value and δ is the Dirac distribution. This corresponds to using the Kramers-Kronig theorem [e.g., *Roddier*, 1971].

As we have seen in the last section, the Green function g_λ is of the form

$$g_\lambda(\underline{x}, t) \sim ||(\underline{x}, t)||^{-h} \tag{41}$$

the scale function $||.||$ acting now on the anisotropic space-time domain. A simple derivation (see Appendix B) confirms that the elliptical dimension $d_{\rm el}$ is indeed the effective dimension of the space-time domain for our process, and therefore

$$\hat{g}_\lambda(\underline{k}, \omega) \sim ||(\underline{k}, \omega)||^{-d_{\rm el}+h} \tag{42}$$

where $d_{\rm el}$ is now:

$$d_{\rm el} \;=\; d \;+\; 1 \;-\; H \tag{43}$$

(d is the spatial dimension). The problem of rendering this Green function causal can indeed be solved by exploiting the arbitrariness of the choice of the scale function $||.||$. Consider

$$||(\underline{x}, t)|| = (|\underline{x}|^{d_{\rm el}-h} + |t|^{\frac{d_{\rm el}-h}{1-H}})^{\frac{1}{d_{\rm el}-h}} \tag{44}$$

with the constraint $d_{\rm el} > h$, and $\underline{x}$ and t are, again, non-dimensionalized ($\underline{x} \mapsto \underline{x}/L$, $t \mapsto t/T$ with L and T the integral scale and time); we assume $L = T = 1$ to simplify the notations. We indeed have

$$||T_\lambda[(\underline{x}, t)]|| = ||(\lambda^{-1}\underline{x}, \lambda^{-(1-H)}t)|| = \lambda^{-1}||(\underline{x}, t)|| \tag{45}$$

We then obtain

$$\hat{g}_\lambda(\underline{k},\omega) \sim \frac{1}{|\underline{k}|^{\frac{d+1}{\chi}} + |\omega|^{\frac{d+1}{\chi(1-H)}}} \tag{46}$$

where

$$\frac{1}{\alpha} + \frac{1}{\chi} = \frac{d_{el}}{d+1} \tag{47}$$

Note that, in the isotropic case $d_{el} = d+1$ we obtain $\chi = \alpha'$, where α' is the usual notation in the universal multifractal litterature ($1/\alpha + 1/\alpha' = 1$). This function can easily be rendered causal, to finally give

$$\hat{g}_\lambda^{\rightarrow}(\underline{k},\omega) \sim \frac{1}{|\underline{k}|^{\frac{d+1}{\chi}} - (i\omega)^{\frac{d+1}{\chi(1-H)}}} \tag{48}$$

and the corresponding equation of diffusion is thus

$$[\partial_t{}^{\xi_1} + (-\Delta)^{\xi_2}]\Gamma_\lambda(\underline{x},t) = \gamma_\lambda(\underline{x},t) \tag{49}$$

where $|\underline{k}|^\beta$ and $(-\Delta)^{\frac{\beta}{2}}$ are a Fourier transform pair, $\xi_1 = \frac{d+1}{\chi(1-H)}$, and $\xi_2 = \frac{d+1}{2\chi}$. This equation can be interpreted as the diffusion of particles (having fractional Lévy flights, a generalization of the fractional Brownian motion to Lévy flights) on a Lévy potential (see Appendix C).

For a purely temporal domain $d = 0$ (no dependence on spatial coordinates), one finds the retarded Green function

$$\hat{g}_\lambda^{\rightarrow}(\omega) \sim (i\omega)^{-\frac{1}{\alpha'}} \tag{50}$$

Note that $\hat{g}_\lambda^{\rightarrow}$ is indeed a restriction of the distribution $p.v.\ (i\omega)^{-\frac{1}{\alpha'}} + \delta(\omega)$ to the range $\omega \in [1/L; \lambda/L]$). In this 1-D temporal case, the generator is indeed a fractional Lévy flight.

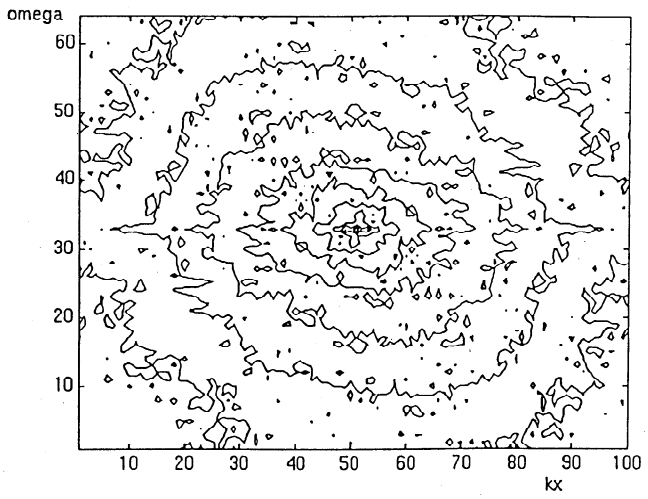

Figure 3. Isocorrelation contours in the Fourier space for the x-t section. The spectrum has been averaged along the y direction. The contours are plotted on a linear scale for the logarithm of the spectrum. They have been shifted so that the center of the figure is indeed the origin.

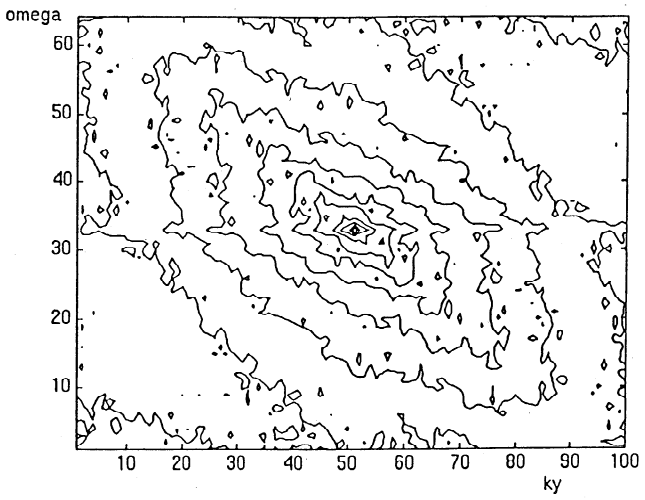

Figure 4. Isocorrelation contours in the Fourier space for the y-t section. The spectrum has been averaged along the x direction. The contours are plotted on a linear scale for the logarithm of the spectrum. They have been shifted so that the center of the figure is indeed the origin.

5. Rainfall Data Analysis

We present here the preliminary results of the analysis of the U.S. composite rainfall data sets derived from NWS radars. We performed this analysis on a portion of the data set, corresponding to a 100×100 square domain in space, for 64 consecutive scans in time. The resolution is 8 km in space and 15 min in time. The mean advecting velocity for this portion was found to be of the order of one pixel for a time step (8 km for 15 min). The rain rates (R) were estimated from the radar reflectivity (Z) using the Marshall-Palmer relation [*Marshall and Palmer*, 1948] with parameters estimated by *Woodley et al.* [1975]: $Z = 300R^{1.4}$, and $Z = Z_e$ where Z_e is the measured "effective" reflectivity (see *Lovejoy et al.* [this issue] for discussion).

We looked at the energy spectra in the Fourier space, for the two 2-D sections x-t and y-t. Following equation (22), we should obtain in the physical space

$$\mathcal{J}^{(1,1)}(\Delta\underline{x},\Delta t) \sim \|(\Delta\underline{x},\Delta t)\|^{-K(2)} \tag{51}$$

since by conservation $K(1) = 0$. Note that this conservation is indeed due to the nature of the data analyzed, i.e., "effective" reflectivity instead of actual rain rates (see *Lovejoy et al.* [this issue] for discussion). Thus, in the Fourier space, as shown in Appendix B, we obtain

$$P(\underline{k},\omega) = \hat{\mathcal{J}}^{(1,1)}(\underline{k},\omega) \sim \|(\underline{k},\omega)\|^{-d_{el}+K(2)} \tag{52}$$

Figures 3 and 4 show the isocorrelation contours in the Fourier space for these two spectra. We can see that the contours have undergone a global "rotation" (indeed a linear transform of coordinates) compared to their expected shape, this transform being due to a trivial anisotropy induced by the overall advection.

Figures 5 and 6 display the 1-D sections $P(k_x)$ for $\omega = 0$ and $P(\omega)$ for $k_x = 0$, and $P(k_y)$ at $\omega = 0$ and $P(\omega)$ at $k_y = 0$, respectively.

It is indeed clear that the algebraic decay in both the space and time directions is observed, in accord with the existence of a scaling space-time cascade process generating the rain field. Moreover, a rough estimate of the scaling anisotropy parameter H is possible using the estimates of the spectral slopes given in figures 5 and 6. Indeed, equation (52) gives, for $\omega = 0$, $P(k) \sim k^{-d_{el}+K(2)}$, and, for $k = 0$, $P(\omega) \sim \omega^{\frac{-d_{el}+K(2)}{1-H}}$. Thus the spectral slopes s_k and s_ω estimated, such that $P(k) \sim k^{-s_k}$ and $P(\omega) \sim \omega^{-s_\omega}$, lead to $H = -0.11$ for the x-t section and $H = -0.09$ for the y-t section. These estimated values of H show a departure from the value 1/3 expected for fully developed turbulence, and also from the estimated $H = 0.5 \pm 0.3$ given in *Lovejoy and Schertzer* [1991] for raindrops. Presumably this discrepancy is related to the the rather small ratio of scale of the data; nevertheless, analyzing techniques were found to be robust, for example when applied to simulated fields involving much larger scale ratios. A more complete and detailed analysis of rainfall data for the determination of this scaling anisotropy parameter is thus needed.

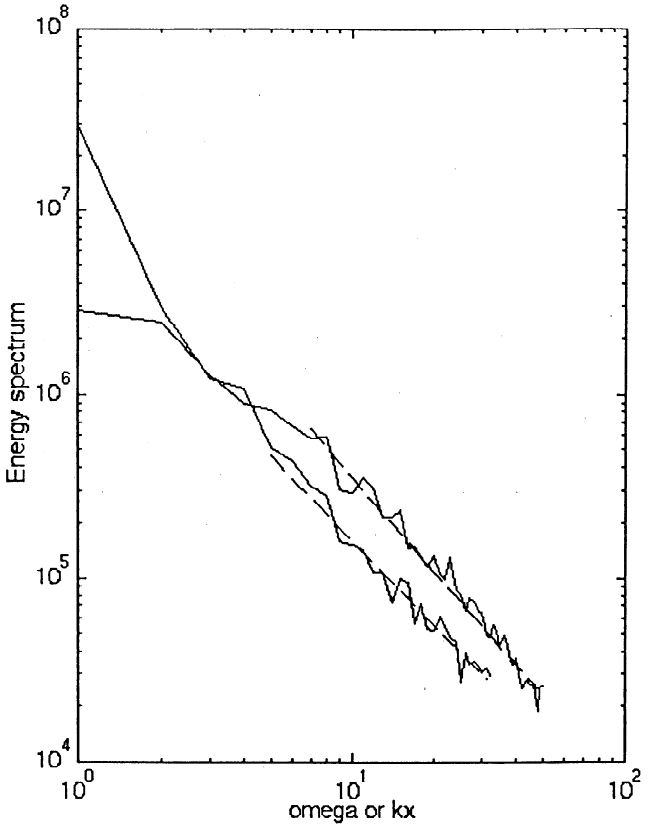

Figure 5. Spectra corresponding to 1-D cut of the k_x-ω density of energy $P(k_x, \omega)$. The two cuts are along the k_x direction at $\omega = 0$ (top) and along the ω direction at $k_x = 0$ (bottom). The estimates of the algebraic slopes, given by the slopes of the dashed lines, are -1.69 for the k_x spectrum, and -1.52 for the ω spectrum.

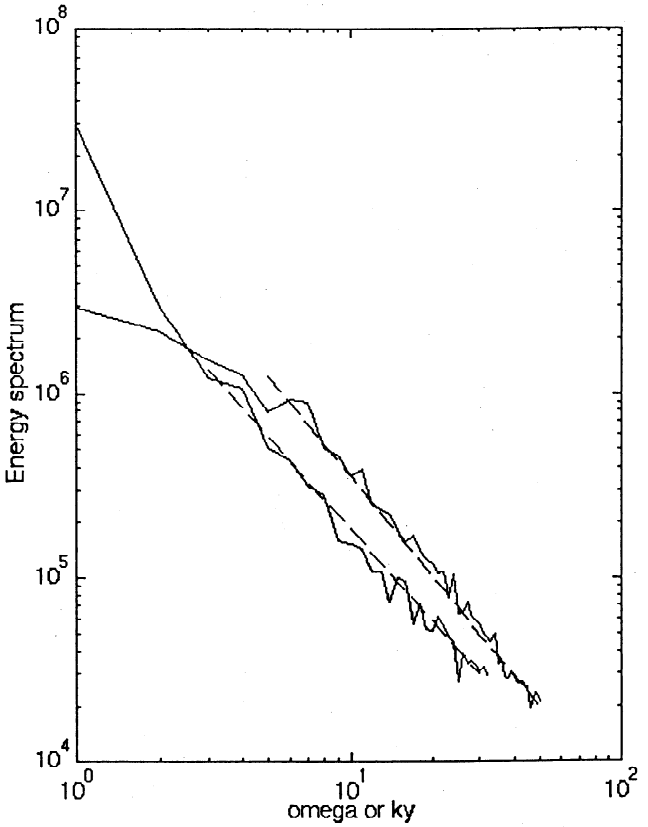

Figure 6. Spectra corresponding to 1-D cut of the k_y-ω density of energy $P(k_y, \omega)$. The two cuts are along the k_y direction at $\omega = 0$ (top) and along the ω direction at $k_y = 0$ (bottom). The estimates of the algebraic slopes, given by the slopes of the dashed lines, are -1.8 for the k_y spectrum, and -1.66 for the ω spectrum.

6. Limit of Predictability and Forecast

A practical application of our space-time model is rainfall forecasts, especially immediate forecasts based on radar maps. But before discussing this central issue, we first have to clarify how much and by how long we can forecast, i.e., what the limits of predictability of our processes are.

Limits of Predictability

Nonlinear systems typically have intrinsic limits of predictability due to their "sensitive dependence on initial conditions". In the case of finite, and especially low-dimensional systems of ODEs, theory (deterministic chaos) has reached a high level of sophistication. In the case of systems with an infinite number of degrees of freedom (nonlinear PDE systems), some similar features are observed or assumed. However, the major difference is that there is a priori no overall characteristic time for these systems, but only for structures of a given spatial scale; therefore the correlation should decay algebraically rather than exponentially. We thus claim that the predictability time τ_l of space-time cascades should increase with scale, following the relation $\tau_l \sim l^{1-H}$, and that the decorrelation follows the al-

gebraic law (22). This specificity of our model indeed recalls the celebrated "butterfly effect" (although usually discussed in the framework of deterministic chaos), classically expected for atmospheric turbulence, and, following our assumptions, for rainfall fields as active scalar fields advected by such a turbulence.

A simple way to discuss this issue more accurately is to simulate two fields initially identical, and decorrelating themselves after a time t_0, as for example a consequence of a perturbation at small scale. Former studies concerning this process have mainly, to our knowledge, dealt with turbulent flows, and, by using closure methods, have obtained similar simulations all giving a typical decorrelation time scaling like $\tau_l \sim l^{\frac{2}{3}}$, not surprisingly following a dimensional argument in every case [*Lorenz*, 1969; *Leith and Kraichnan*, 1972; *Métais and Lesieur*, 1986].

Figure 7 displays the cross-correlation spectra at different times t corresponding to the following simulation: we took two fields $\epsilon_{1\lambda}$ and $\epsilon_{2\lambda}$ having subgenerator fields $\gamma_{1\lambda}$ and $\gamma_{2\lambda}$ such that

$$\begin{array}{l} \gamma_{1\lambda}(x,t) = \gamma_{2\lambda}(x,t)\ \forall t < t_0 \\ \gamma_{1\lambda}(x,t) \text{ and } \gamma_{2\lambda}(x,t) \text{ independent } \forall t \geq t_0 \end{array} \tag{53}$$

For this simulation the exponent H is taken equal to -1, $\alpha = 1.8$, $d = 1$, and the size of the grid is 256×256. The value of $K(2)$ is 0.26 (C_1, i.e., the codimension of the mean singularity, is equal to 0.14). We compute the spectra

$$E_W(k,t) = |\langle \hat{\epsilon}_{1\lambda}(k,t)\hat{\epsilon}_{2\lambda}(k,t)\rangle| \tag{54}$$

for different times $t - t_0 = n\tau_{l_{\min}}$, where $\tau_{l_{\min}}$ is the turn-over time at the minimal scale, and $n = \{0, 10, 20\}$. The ensemble average is performed on 32 realizations. We indicate on the graph the estimates of the algebraic slopes β (depending on t) of the spectra, so that

$$E_W(k,t) \sim k^{-\beta} \tag{55}$$

in the inertial range (decreasing in length with t). It can be observed that the phenomenology of the cascade, i.e,. with smaller structures possessing shorter lifetimes compared to bigger structures, is indeed retrieved here, with a stronger decorrelation rate at smaller scales. Also, we observe the apparition of a cut-off wavenumber $k_e(t)$, scaling like $k_e(t) \sim t^{\frac{-1}{1-H}}$, and corresponding to the smallest predictable scale at time t. We detail in Appendix D the expectations for such spectra, i.e., the changes in the inertial range and in the algebraic slope.

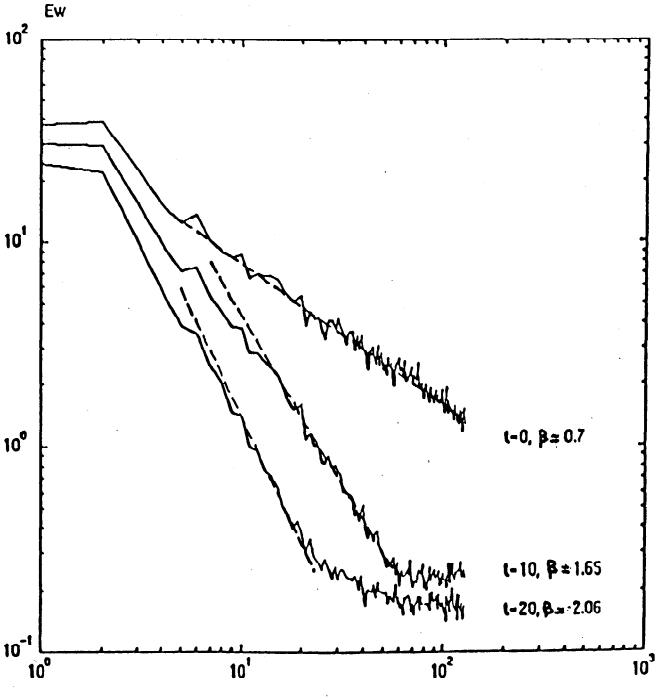

Figure 7. Cross-correlation spectra for two diverging fields. Parameters are $\alpha = 1.8$, $d = 1$, $K(2) = 0.26$. See text for more details.

Forecast

As stated earlier, to define a multifractal forecast method is one of the major goals of this paper. The understanding of rainfall fields as ensembles of interwoven structures at all scales, characterized dynamically by lifetimes scaling like $\tau_l \sim l^{1-H}$, leads to an intuitive picture of an optimally (in the sense of not creating artificial information, i.e., not generating structures at scales smaller than the smallest predictable scale) predicted rain field knowing its states in the past. Clearly, since all information about a given structure after a period longer than its lifetime is lost, we should predict that this structure completely vanish. In the meantime, the predicted states should consider this structure to undergo a relatively constant modulation. We thus see that there is a clear link between the limits of predictability and the behavior of this predictor (see Appendix D for a more formal discussion). This is a natural link, since the limit of predictability acts like a boundary mark for the predictor, i.e., past the predictability time associated with the structures at a given scale, these structures are simply "erased" for the predictor, since nothing is known about them. This confirms that one needs to know the field on larger and larger scales in order to predict its future at longer and longer intervals.

In the preceding sections, the construction of $\epsilon_\lambda(\underline{x}, t)$ was built up starting from a white noise field, the subgenerator $\gamma_\lambda(\underline{x}, t)$. The whole construction can be summarized by the action of a transform Ω_λ, depending on the parameters d, α, H and λ, on the subgenerator:

$$\epsilon_\lambda = \Omega_\lambda[\gamma_\lambda] \tag{56}$$

By inverting this transform, one can determine the subgenerator associated with a given multifractal field. Note however that rather complex and interesting effects can appear, since the direct transform involves a construction going from the large scales down to the small scales, thus without any divergence problems (i.e., generating a "bare" quantity) while the inverse transform on ϵ_λ requires some spatial average of an intermittent field, thus possessing divergent moments of large

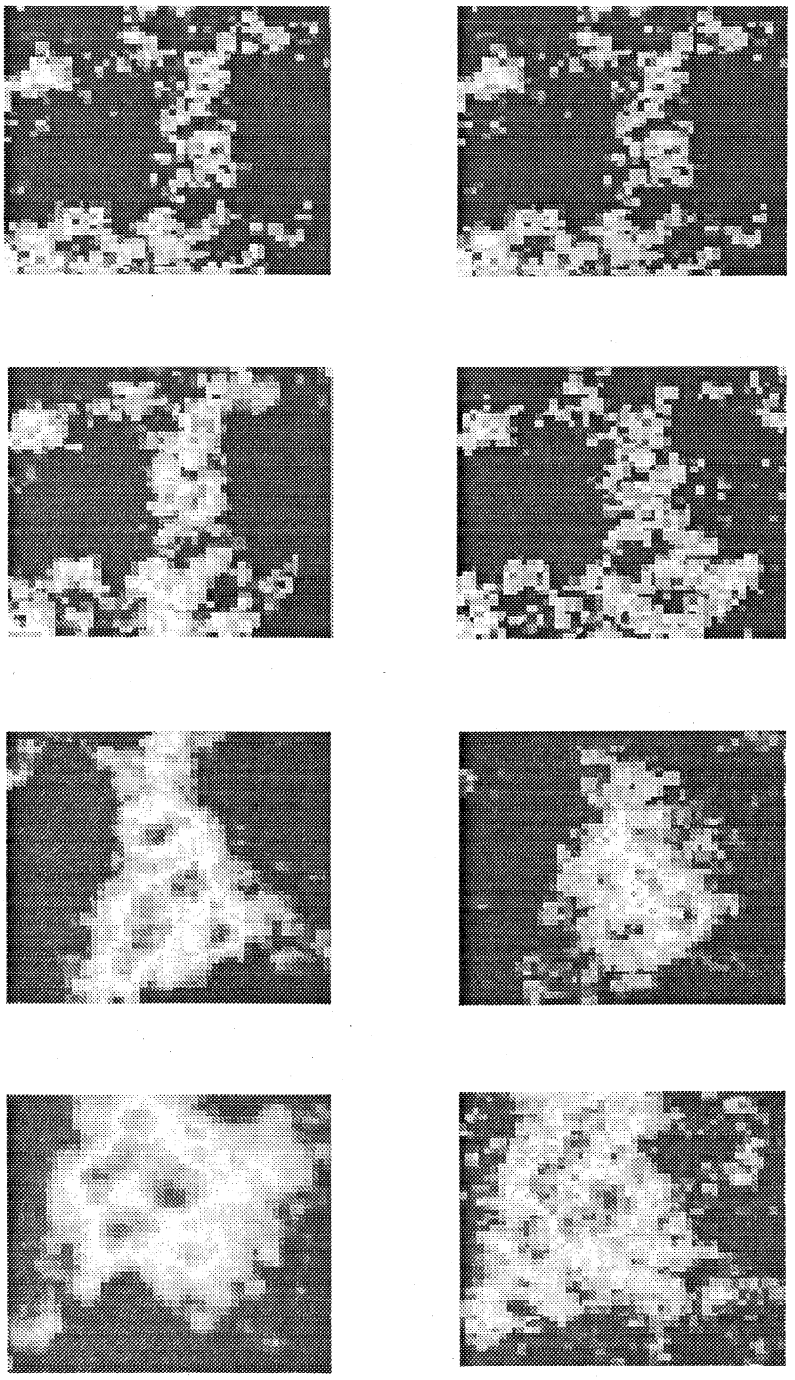

Figure 8. Optimal predictor compared to the actual future states for a realization with parameters $\alpha = 1.8$, $H = \frac{1}{3}$, $d = 2$, and $C_1 = 0.08$. We display the optimal predictor on the left column, and the actual field on the right. The scans shown correspond thus to 2-D spatial scans taken at times $n = 0, 2, 10, 20$ (from top to bottom). See text for more details.

enough order due to the presence of extremely strong singularities (i.e., a "dressed" quantity). See *Schertzer and Lovejoy* [1987a] for a more detailed discussion.

Knowing the process $\epsilon_\lambda(\underline{x}, t)$ for times $t < t_0$, we are thus able to compute the field $\gamma_\lambda(\underline{x}, t)$ up to this time t_0. The requirements for our predictor are that (1) the predicted field, at any given time, should satisfy the same normalization conditions as the ones verified by the known physical field, (2) it should respect the limits of predictability described above, therefore it should be truncated in the Fourier space around the cut-off wavenumber $k_e(t)$, and (3) it should obviously result from a causal process. This predictor is obtained by choosing a subgenerator γ' such that

$$\begin{aligned} \gamma'_\lambda(\underline{x}, t) &= \gamma_\lambda(\underline{x}, t) \ \forall t < t_0 \\ \gamma'_\lambda(\underline{x}, t) &= 0 \ \forall t \geq t_0 \end{aligned} \tag{57}$$

without expliciting the normalization condition. This

choice for γ' can also be understood by recalling that γ is a white noise field (by definition), and since no information is available for the subgenerator at times $t > t_0$, to take $\gamma' = 0$ in the future is natural.

The last step is then to apply Ω_λ on this new subgenerator, to finally obtain the predicted $\epsilon'_\lambda(\underline{x}, t)$ such that

$$\begin{array}{l} \epsilon'_\lambda(\underline{x}, t) = \epsilon_\lambda(\underline{x}, t) \ \forall t < t_0 \\ \epsilon'_\lambda(\underline{x}, t) \text{ predicted } \forall t \geq t_0 \end{array} \tag{58}$$

It is important to note that this procedure is made possible only because the causality of Ω_λ, and thus of our model, is respected, so that the future does not interfere with the known field $\epsilon_\lambda(\underline{x}, t)$ (for $t < t_0$); otherwise, a noncausal Ω_λ would lead to a field $\epsilon'_\lambda(\underline{x}, t)$ different from $\epsilon_\lambda(\underline{x}, t)$ for $t < t_0$.

We have simulated this procedure for the parameters $d = 2$ (two spatial coordinates, one temporal coordinate), $\alpha = 1.8$, $H = 1/3$, $C_1 = 0.08$, on a cubic grid of size 64^3. We display our results in Figure 8, comparing the predictor (left column) with the actual future states (right column), for times $t - t_0 = n\tau_{l_{\min}}$ with $n = \{2, 10, 20\}$. We have brought all the negative singularities to $-\infty$, since small enough, negative singularities lead, for $\lambda >> 1$, to "holes" in the field, giving zero values for the rainfall field as seen by a measuring apparatus.

7. Conclusions

We follow in this paper the natural link widely used in carlier cascade models of rainfall: the scaling of the turbulent medium leads to similar symmetries for the advected scalar field. By looking at the scaling in both space and time, we claim that rain fields are indeed the result of space-time multiplicative cascades. This leads us to propose a model of continuous cascades respecting causal properties. The process corresponds thus to scaling dynamics and, phenomenologically, to a cascade of structures at all scales characterized by scaling lifetimes. We propose a very straightforward approach to the understanding of the loss of predictability for this process and, correspondingly, a method to predict its future states.

A complete and intensive analysis of rainfall data is the next step in our work, the preliminary results being rather promising.

Appendix A

In this appendix we summarize an important property of universal continuous cascade processes (see also *Schertzer and Lovejoy* [1991]). Equation (24) with the choice of a scaling filter band-limited to $|\underline{k}| \in [1/L; \lambda/L]$ leads to

$$\Gamma_\lambda(\underline{x}) = \int_{\mathcal{D}_\lambda} d\underline{x}' \ |\underline{x}'|^{-h} \ \gamma_\lambda(\underline{x} - \underline{x}') \tag{A1}$$

where the integration domain $\mathcal{D}_\lambda : \{|\underline{x}'| \in [L/\lambda; L]\}$ is the consequence of the band limitation constraint on the filter. $\Gamma_\lambda(\underline{x})$ is then a sum of independent stable random variables; recalling the stability property of a Lévy random variable γ of index α,

$$\sum_{i=1}^{n} a_i \gamma_i \equiv (\sum_{i=1}^{n} |a_i|^\alpha)^{\frac{1}{\alpha}} \gamma + b_n \tag{A2}$$

where all the γ_i and γ are identically distributed (and the γ_i are all independent), and b_n is a recentering term, we then have

$$\Gamma_\lambda(\underline{x}) \equiv (\int_{\mathcal{D}_\lambda} d\underline{x}' \ |\underline{x}'|^{-\alpha h})^{\frac{1}{\alpha}} \gamma + \gamma_0 \tag{A3}$$

with γ an α-stable random variable and γ_0 a recentering term. This finally gives

$$\langle e^{q\Gamma_\lambda(\underline{x})} \rangle = \langle \exp[(q^\alpha \int_{\mathcal{D}_\lambda} d\underline{x}' \ |\underline{x}'|^{-\alpha h})^{\frac{1}{\alpha}} \gamma + q\gamma_0] \rangle \tag{A4}$$

and

$$\langle e^{q\Gamma_\lambda(\underline{x})} \rangle = \exp[q^\alpha \int_{\mathcal{D}_\lambda} d\underline{x}' \ |\underline{x}'|^{-\alpha h} + q\gamma_0] \tag{A5}$$

Appendix B

We give here some technical details concerning the Fourier transform of the scale function $||.||$ introduced in GSI (see equation (34)), and involved in the calculation of the Green function of equation (41) (see also *Pflug et al.* [1993]). Consider the function

$$f_\beta(\underline{X}) \sim ||\underline{X}||^{-\beta} \tag{B1}$$

where $\underline{X}$ is the vector in the space time domain $\underline{X} = (\underline{x}, t)$. We determine its Fourier transform:

$$\hat{f}_\beta(\underline{K}) = \int d\underline{X} \ ||\underline{X}||^{-\beta} e^{i\underline{K}\cdot\underline{X}} \tag{B2}$$

The change of coordinate $\underline{X} = T_\lambda[\underline{Y}]$ gives

$$\hat{f}_\beta(\underline{K}) = \int (\lambda^{-\mathcal{G}} \cdot d\underline{Y}) \ ||T_\lambda[\underline{Y}]||^{-\beta} e^{i\underline{K}\cdot T_\lambda[\underline{Y}]} \tag{B3}$$

Given that $\lambda^{-\mathcal{G}} d\underline{Y} = \lambda^{-d} d\underline{Y} \lambda^{-(1-H)} dt = \lambda^{-d_{el}} d\underline{Y}$ ($\lambda^{-d_{el}}$ is thus the Jacobian of the transformation), we obtain

$$\hat{f}_\beta(\underline{K}) = \int d\underline{Y} \ \lambda^{-d_{el}} \lambda^\beta \ ||\underline{Y}||^{-\beta} e^{i\underline{K}\cdot T_\lambda[\underline{Y}]} \tag{B4}$$

It is easy to check that $\underline{K}\cdot T_\lambda[\underline{Y}] = {}^t T_\lambda[\underline{K}]\cdot\underline{Y}$, where ${}^t T_\lambda$ is the transpose of the scale changing operator (${}^t T_\lambda = T_\lambda$ in our self-affine case), and thus

$$\hat{f}_\beta(\underline{K}) = \lambda^{\beta - d_{el}} \int d\underline{Y} \ ||\underline{Y}||^{-\beta} e^{i T_\lambda[\underline{K}]\cdot\underline{Y}} \tag{B5}$$

$$= \lambda^{\beta - d_{el}} \hat{f}_\beta(T_\lambda[\underline{K}]) \tag{B6}$$

which finally gives

$$\hat{f}_\beta(\underline{K}) \sim ||\underline{K}||^{-d_{el}+\beta} \quad \text{(B7)}$$

Appendix C

Using the same arguments as those detailed by *Chechkin et al.* [1995], we can show that the equation of diffusion

$$[\partial_t{}^{\xi_1} + (-\Delta)^{\xi_2}]\ \Gamma_\lambda(\underline{x},t) = \gamma_\lambda(\underline{x},t) \quad \text{(C1)}$$

is the Fokker-Planck equation with corresponding Langevin equation of the form:

$$\frac{d^{\xi_1}\underline{x}(t)}{dt^{\xi_1}} = \underline{\zeta}(t) \quad \text{(C2)}$$

where $\underline{\zeta}(t)$ is a vectorial, symmetrical Lévy white noise (since the spatial operator is symmetrical) of Lévy index $\xi_2 = (d+1)/2\chi$; the constraint $d_{el} > h$ ensures $\xi_2 > 0$, and taking $H = 1/3$ and $\alpha \geq 1$ ensures $\xi_2 \leq 2, \forall d$. Note that α has been estimated to 1.35 for rainfall data [*Tessier et al.*, 1993]. Equation (C1) corresponds thus to the diffusion of particles with fractional Lévy motions undergoing the action of the "source" $\gamma_\lambda(\underline{x},t)$ (or "sink" when $\gamma_\lambda(\underline{x},t) < 0$). We can then write a very formal solution in terms of path integrals:

$$\Gamma_\lambda(\underline{x},t) = \int d\underline{\mathcal{L}}\ \Gamma_\lambda(\underline{x} - \underline{\mathcal{L}}(t-\tau), t-\tau) \int_0^\tau dt' \gamma_\lambda(\underline{x} - \underline{\mathcal{L}}(t'), t-t') \quad \text{(C3)}$$

where $\underline{\mathcal{L}}$ is a fractional Lévy flight of dimension d verifying equation (C2) starting at $\underline{x} = 0$ at $t = 0$, the integration $\int d\underline{\mathcal{L}}$ then corresponds to a renormalized sum on all the paths. The propagator giving the generator at a time t knowing its state at time $t - \tau$ (and knowing also the subgenerator form $t - \tau$ until t) thus corresponds to an infinite number of particles undergoing fractional Lévy flights on a Lévy potential (the subgenerator).

Appendix D

In this appendix we look at the links between different correlation functions corresponding to different schemes; the theoretical development for determining the exact correlated energy spectrum is given in *Marsan et al.* [1996] and D. Schertzer et al., Multifractal cascade dynamics and turbulent intermittency, submitted to *Fractals*, 1996. We show here that the three correlation functions,

$$Y_1(\Delta\underline{x}, \Delta t) = \langle \epsilon_\lambda(\underline{x},t)\ \epsilon_\lambda(\underline{x}+\Delta\underline{x}, t+\Delta t)\rangle \quad \text{(D1)}$$

for a given causal field $\epsilon_\lambda(\underline{x},t)$,

$$Y_2(\Delta\underline{x}, \Delta t) = \langle \epsilon'_\lambda(\underline{x}, t_0+\Delta t)\ \epsilon'_\lambda(\underline{x}+\Delta\underline{x}, t_0+\Delta t)\rangle \quad \text{(D2)}$$

for a field $\epsilon'_\lambda(\underline{x},t)$ corresponding to a subgenerator γ'_λ verifying (57), i.e., with $\gamma'_\lambda(\underline{x},t) = 0$ for $t \geq t_0$, and

$$Y_3(\Delta\underline{x}, \Delta t) = \langle \epsilon_{1\lambda}(\underline{x}, t_0+\Delta t)\ \epsilon_{2\lambda}(\underline{x}+\Delta\underline{x}, t_0+\Delta t)\rangle \quad \text{(D3)}$$

for two fields such that their subgenerators $\gamma_{1\lambda}$ and $\gamma_{2\lambda}$ verify (53) (i.e. $\gamma_{1\lambda}(\underline{x},t) = \gamma_{2\lambda}(\underline{x},t)$ for $t < t_0$) all have identical behaviors in time, and we predict the temporal evolution of the shape of their spatial Fourier transforms.

Y_1 is simply given by equation (22) which can be simplified to

$$Y_1(\Delta\underline{x}, \Delta t) \sim ||(\Delta\underline{x}, \Delta t)||^{-K(2)} \quad \text{(D4)}$$

In order to determine Y_2, we single out the scale l such that $\Delta t = \tau_l$; thus $l = \Delta t^{\frac{1}{1-H}}$ (again, we nondimensionalize $\underline{x}$ and t using the integral scale/time). Then for all the structures at scales $|\Delta\underline{x}| > l$, the correlation function Y_2 is still unchanged, since the lifetimes of these structures are longer than the interval Δt considered. The correlation is thus simply

$$Y_2(\Delta\underline{x}, \Delta t) \sim |\Delta\underline{x}|^{-K(2)},\ \forall |\Delta\underline{x}| > \Delta t^{\frac{1}{1-H}} \quad \text{(D5)}$$

On the contrary, the scales $|\Delta\underline{x}| < l$ have been spoiled by the null values, since all the structures at those scales have been changed, and have thus undergone the influence of the null part of the subgenerator; we then have

$$Y_2(\Delta\underline{x}, \Delta t) \sim |\Delta t|^{-\frac{K(2)}{1-H}},\ \forall |\Delta\underline{x}| < \Delta t^{\frac{1}{1-H}} \quad \text{(D6)}$$

We then find the same result as for Y_1, by using the proper scale function $||.||$ (for example, $||(\underline{x},t)|| = \max\{|\underline{x}|, t^{\frac{1}{1-H}}\}$). Finally, the same handwaving argumentation can be used for Y_3, and we find $Y_1 \sim Y_2 \sim Y_3$. The spatial Fourier transform of Y_1 gives

$$\langle \hat{\epsilon}_\lambda(\underline{k},t)\ \hat{\epsilon}_\lambda(-\underline{k}, t+\Delta t)\rangle = \int\int d\underline{x}\ d\Delta\underline{x}\ e^{-i\underline{k}\Delta\underline{x}} \langle \epsilon_\lambda(\underline{x},t)\ \epsilon_\lambda(\underline{x}+\Delta\underline{x}, t+\Delta t)\rangle \quad \text{(D7)}$$

$$\sim \int d\Delta\underline{x}\ e^{-i\underline{k}\Delta\underline{x}}\ ||(\Delta\underline{x}, \Delta t)||^{-K(2)} \quad \text{(D8)}$$

For $\Delta t = 0$, we thus find

$$\hat{Y}_1(\underline{k},t) \sim |\underline{k}|^{-d+K(2)} \quad \text{(D9)}$$

For $\Delta t > 0$, the breaking of scaling in the integral in (D8) at $|\Delta\underline{x}| \sim \Delta t^{\frac{1}{1-H}}$ leads to an equivalent breaking in the Fourier space around $|\underline{k}| = k_e(\Delta t) \sim \Delta t^{-\frac{1}{1-H}}$, thus reducing the inertial range. In the limit case $\Delta t \to \infty$ the function to be integrated in (D8) tends to zero, and the correlation is thus found to be null at every wavenumber.

Acknowledgments. The authors wish to thank Y. Chigirinskaia, C. Naud, S. Pecknold, F. Schmitt, and Y. Tessier for helpful comments, discussions, and technical assistance, and D. Kwak and L. Maples for correcting the English. We also are very grateful to the people at the Users Services Office of the EOSDIS MSFC DAAC, who helped us by making their database readily accessible. Partial support by INTAS-93-1194 contract is gratefully acknowledged.

References

Austin, P. M., and R. A. Houze, Analysis of structure of precipitation patterns in New England, *J. Appl. Meteorol.*, *11*, 926-935, 1972.

Benzi, R., G. Paladin, G. Parisi, and A. Vulpiani, On the multifractal nature of fully developed turbulence, *J. Phys. A*, *17*, 3521-3531, 1984.

Brenier, P., D. Schertzer, A. Davis, G. Sarma, S. Lovejoy, and D. Lavallée, Multifractal dynamics. Météo France-C2VR-INRIA, 1991. Distributed with *Cellular Automata: Prospects in Astronomy and Astrophysics*, edited by J. M. Perdang and A. Lejeune, World Sci., River Edge, N. J., 1991.

Cates, M. E., and J. M. Deutsch, Spatial correlations in multifractals, *Phys. Rev. A*, *35*(11), 4907-4910, 1987.

Chechkin, A.V., D. Schertzer, A. V. Tur, and V. V. Yanovsky, Generalized Fokker- Planck equation for anomalous diffusion, *Ukr. J. Phys.*, *40*(5), 434-439, 1995.

Corrsin, S., On the spectrum of isotropic temperature fluctuations in an isotropic turbulence, *J. Appl. Phys.*, *22*, 469, 1951.

Frisch, U., P. L. Sulem, and M. Nelkin, A simple dynamical model of intermittency in fully developed turbulence, *J. Fluid Mech.*, *87*, 719, 1978.

Grassberger, P., Generalized dimensions of strange attractors, *Phys. Lett. A*, *97*, 227, 1983.

Halsey, T.C., M. H. Jensen, L. P. Kadanoff, I. Procaccia, and B. Shraiman, Fractal measures and their singularities: The characterization of strange sets, *Phys. Rev. A*, *33*, 1141, 1986.

Hentschel, H. G. E., and I. Proccacia, The infinite number of generalized dimensions of fractals and strange attractors, *Phys. D*, *8*, 435, 1983.

Kahane, J. P., Sur le chaos multiplicatif, *Ann. Sci. Math. Quebec*, *9*, 435, 1985.

Kolmogorov, A. N., Local structure of turbulence in an incompressible liquid for very large Reynolds numbers, *Dokl. Acad. Sci. USSR.*, *30*, 299, 1941.

Kolmogorov, A. N., A refinement of previous hypotheses concerning the local structure of turbulence in viscous incompressible fluid at high Reynolds number, *J. Fluid Mech.*, *83*, 349, 1962.

Leith, C.E., and R. H. Kraichnan, Predictability of turbulent flows, *J. Atmos. Sci.*, *29*, 1972.

Lorenz, E. N., The predictability of a flow which possesses many scales of motion, *Tellus*, *21*, 289, 1969.

Lovejoy, S., and B. Mandelbrot, Fractal properties of rain and a fractal model, *Tellus*, *37*, 209, 1985.

Lovejoy, S., and D. Schertzer, Generalized scale invariance and fractal models of rain, *Water Resour. Res.*, *21*(8), 1233, 1985.

Lovejoy, S., and D. Schertzer, Multifractal analysis techniques and the rain and cloud fields from 10^{-3} to 10^{6} m, in *Non-Linear Variability in Geophysics*, edited by D. Schertzer and S. Lovejoy, pp. 111-144, Kluwer Acad., Norwell, Mass., 1991.

Lovejoy, S., and D. Schertzer, Multifractals and rain, in *New Uncertainty Concepts in Hydrology and Hydrological Modeling*, edited by A. W. Kundzewicz, p. 61, Cambridge Univ. Press, New York, 1995.

Lovejoy, S., D. Schertzer, and K. Pflug, Generalized scale invariance and differential rotation in cloud radiances, *Phys. A*, *185*, 121-128, 1992.

Lovejoy, S., M. R. Duncan and D. Schertzer, The scalar multifractal radar observer's problem, *J. Geophys. Res.*, in this issue.

Mandelbrot, B., Intermittent turbulence in self-similar cascades: Divergence of high moments and dimension of the carrier, *J. Fluid Mech.*, *62*, 331, 1974.

Mandelbrot, B., *The Fractal Geometry of Nature*, W. H. Freeman, New York, 1982.

Marsan, D., D. Schertzer, and S. Lovejoy, Predictability of multifractal processes: The case of turbulence, to appear in *Proceedings of the CFIC Conference*, edited by G. Biardi, M. Giona and A. R. Giona, World Sci., Singapore, 1996.

Marshall, J. S., and W. M. Palmer, The distribution of raindrops with size, *J. Meteorol.*, *5*, 165, 1948.

Meneveau, C., and K. R. Sreenivasan, Simple multifractal cascade model for fully developed turbulence, *Phys. Rev. Lett.*, *59*(13), 1424, 1987.

Métais, O., and M. Lesieur, Statistical predictability of decaying turbulence, *J. Atmos. Sci.*, *43*(9), 1986.

Monin, A. S., and A. M. Yaglom, *Statistical Fluid Mechanics: Mechanics of Turbulence*, edited by J. L. Lumley, MIT Press, Cambridge, Mass., 1975.

Novikov, E. A., and R. Stewart, Intermittency of turbulence and spectrum of fluctuations in energy-dissipation, *Izv. Akad. Nauk. SSSR Ser. Geofiz.*, *3*, 408, 1964.

Obukhov, A., Spectral energy distribution in a turbulent flow, *Dokl. Akad. Nauk. SSSR*, *32*(1), 22-24, 1941.

Obukhov, A., Structure of the temperature field in a turbulent flow, *Izv. Akad. Nauk. SSSR Geogr. Geofiz.*, *13*, 55, 1949.

Obukhov, A., Some specific features of atmospheric turbulence, *J. Fluid. Mech.*, *13*, 77, 1962.

O'Neil, J., and C. Meneveau, Spatial correlations in turbulence: Predictions from the multifractal formalism and comparison with experiments, *Phys. Fluid A*, *5*(1), 158, 1993.

Parisi, G., and U. Frisch, A multifractal model of intermittency, in *Turbulence and Predictability in Geophysical Fluid Dynamics and Climate Dynamics*, edited by M. Ghil, R. Benzi, and G. Parisi, p. 84, North-Holland, New York, 1985.

Pecknold, S., S. Lovejoy, D. Schertzer, C. Hooge, and J. F. Malouin, The simulation of universal multifractals, in *Cellular Automata: Prospects in Astronomy and Astrophysics*, edited by J. M. Perdang and A. Lejeune, pp. 228-267, World Sci., River Edge, N. J., 1993.

Pecknold, S., S. Lovejoy, and D. Schertzer, The morphology and texture of anisotropic multifractals using generalized scale invariance, in *Stochastic Models in Geosystems, IMA Math. Ser.*, edited by S. S. Molchan and W. A. Woyczynski, Springer-Verlag, New York, in press, 1996.

Pflug, K., S. Lovejoy, and D. Schertzer, Generalized scale invariance, differential rotation and cloud texture: Analysis and simulation, *J. Atmos. Sci.*, *50*, 538-553, 1993.

Pietronero, L., and A. P. Siebesma, Self-similarity of fluctuations in random multiplicative processes, *Phys. Rev. Lett.*, *57*, 1098, 1986.

Roddier, F., *Distributions et Transformation de Fourier*, Ediscience, Paris, 1971.

Schertzer, D., and S. Lovejoy, On the dimension of atmospheric motions, in *Turbulence and Chaotic Phenomena in Fluids*, edited by T. Tatsumi, pp. 505-508, North-Holland, New York, 1984.

Schertzer, D., and S. Lovejoy, Generalized scale invariance in turbulent phenomena, *Phys. Chem. Hydrodyn. J.*, *6*, 623-635, 1985.

Schertzer, D., and S. Lovejoy, Physical modeling and analysis of rain and clouds by anisotropic scaling and multiplicative processes, *J. Geophys. Res.*, *92*(D8), 9693-9714, 1987a.

Schertzer, D., and S. Lovejoy, Singularités anisotropes, divergences des moments en turbulence: Invariance d'échelle généralisée et processus multiplicatifs, *Ann. Sci. Math. Quebec*, *11*(1), 139-181, 1987b.

Schertzer, D., and S. Lovejoy, Generalized scale invariance and multiplicative processes in the atmosphere, *Pure Appl. Geophys.*, *130*, 209-244, 1989.

Schertzer, D., and S. Lovejoy, Scaling nonlinear variability in geodynamics: Multiple singularities, observables and universality classes, in *Nonlinear Variability in Geophysics: Scaling and Fractals*, edited by D. Schertzer and S. Lovejoy, pp. 41-82, Kluwer Acad., Norwell, Mass., 1991.

Schertzer, D., and S. Lovejoy, Hard and soft multifractal processes, *Phys. A*, *185*, 187-194, 1992.

Tessier, Y., S. Lovejoy, and D. Schertzer, Universal multifractals in rain and clouds: Theory and observations, *J. Appl. Meteorol.*, *32*(2), 223-250, 1993.

Waymire, E., V. K. Gupta, and I. Rodriguez-Iturbe, A spectral theory of rainfall intensity at the meso-beta scale, *Water Resour. Res.*, *20*, 1453-1465, 1984.

Wilson, J., S. Lovejoy, and D. Schertzer, Physically based cloud modelling by multiplicative cascade processes, in *Nonlinear Variability in Geophysics: Scaling and Fractals*, edited by D. Schertzer and S. Lovejoy, pp. 185-208, Kluwer Acad., Norwell, Mass., 1991.

Woodley, W. L., A. R. Olsen, A. Herndon, and V. Wiggert, Comparison of gage and radar methods of convective rain measurement, *J. Appl. Meteorol.*, *14*, 909, 1975.

Yaglom, A. M., The influence of the fluctuation in energy dissipation on the shape of turbulent characteristics in the inertial interval, *Sov. Phys. Dokl.*, *2*, 26, 1966.

S. Lovejoy, Physics Department, Mc Gill University, 3600 University Street, Montreal, Quebec H3A 2T8, Canada. (e-mail: lovejoy@physics.mcgill.ca)

D. Marsan and D. Schertzer, Laboratoire de Météorologie Dynamique, Université Pierre et Marie Curie, BP 99, 4 Place Jussieu, 75252 Paris Cedex 05, France.(e-mail: marsan@lmd.jussieu.fr, schertzer@lmd.jussieu.fr)

(Received December 21, 1995; revised May 22, 1996; accepted May 28, 1996.)